Topology of the postperovskite phase transition and mantle dynamics

Marc Monnereau*† and David A. Yuen‡

*Unité Mixte de Recherche 5562, Centre National de la Recherche Scientifique–Université Paul Sabatier Toulouse III, 14 Avenue Edouard Belin, 31400 Toulouse, France; and ‡Department of Geology and Geophysics and Minnesota Supercomputing Institute, University of Minnesota, Minneapolis, MN 55455-0219

Edited by Russell J. Hemley, Carnegie Institution of Washington, Washington, DC, and approved March 30, 2007 (received for review September 16, 2006)

The postperovskite (ppv) phase transition occurs in the deep mantle close to the core–mantle boundary (CMB). For this reason, we must include in the dynamical considerations both the Clapeyron slope and the temperature intercept, T_{int}, which is the temperature of the phase transition at the CMB pressure. For a CMB temperature greater than T_{int}, there is a double crossing of the phase boundary by the geotherms associated with the descending flow. We have found a great sensitivity of the shape of the ppv surface due to the CMB from variations of various parameters such as the amount of internal heating, the Clapeyron slope, and the temperature intercept. Three-dimensional spherical models of mantle convection that can satisfy the seismological constraints depend on the Clapeyron slope. At moderate value, 8 MPa/K, the best fit is found with a core heat flow amounting for 40% of the total heat budget (≈15 TW), whereas for 10 MPa/K the agreement is for a lower core heat flow (20%, ≈7.5 TW). In all cases, these solutions correspond to a temperature intercept 200 K lower than the CMB temperature. These models have holes of perovskite adjacent to ppv in regions of hot upwellings.

D″ layer | Clapeyron slope | temperature intercept | mantle convection | spherical model

The recent discovery of the postperovskite (ppv) transition (1–3) has provoked an immense interest in the earth sciences because of the close proximity of the phase change to the core–mantle boundary (CMB), unveiling a large part of the enigmatic D″ layer. The D″ is a seismic structure whose complexity has remained puzzling for a long time. Interpreted in terms of phase boundary undulations, it would offer the chance to provide an absolute constraint on the temperature within the thermal boundary layer of the mantle. This would have great impact on our understanding of the dynamical state and thermal history of the earth. Concerted efforts recently have been devoted to sharpening the seismic imaging of D″ (4–6), but results remain interpreted in the framework of 1D thermal models. On the other hand, previous work (7–11) investigating mantle convection with a ppv transition has focused more on dynamical effects and the magnitude of the Clapeyron slope than on the topology of the ppv surface itself. Thus, these investigators have neglected to consider the temperature intercept of the phase transition, which matters a lot in the case of a ppv transition because it is situated so near to the lower boundary of mantle convection.

This delicate location makes it necessary for one to take into account the relative magnitude between the temperature at the CMB, T_{CMB}, and the temperature of the ppv transition at the CMB pressure of 135 GPa. This latter temperature is called the temperature intercept, T_{int} (see Fig. 1). In Fig. 1, we show the relationship between various geotherms (cold, warm, and hot) and the phase boundary, commonly known as the Clapeyron curve (red color), which is given by the equation cast in red. We note that in the case when T_{CMB} is greater than T_{int}, the geotherm may cross the phase boundary at two places (known as "double-crossing") (4). This feature is necessarily related to the existence of hotter regions where the geotherm cannot cross the phase change. In such a case, the core will be partially covered by lenses of ppv whose topology may be complex. For $T_{CMB} < T_{int}$, no double-crossing is possible, and the ppv will constitute a continuous layer, just thicker in colder regions of the deep mantle.

Our knowledge of the D″ topology is largely incomplete. However, because there is accumulating seismic and mineral physical evidence pointing to the dominating phase-change nature of the D″ region (12, 13), any local information on D″ topography may provide a global constraint on the core–mantle thermal boundary layer. For instance, the recent seismological discovery of a possible double crossing (4) would fix a lower bound for T_{CMB}, i.e., T_{int}, completely independent from the one provided by the melting curve of iron (14). Despite active research, a large uncertainty still remains in the determination of these thermodynamical parameters, especially for the temperature intercept. First-principles calculations and high-pressure experiments based on MgO pressure scale have definitively shown that this mineral transition is strongly exothermic with a Clapeyron slope ranging from 7 to 11.5 MPa/K (see ref. 15 for a review). The pressure of the transition at 2,500 K is estimated to be between 117 and 130 GPa, so that T_{int} would lie between 3,200 and 5,000 K.

Here, we wish to assess these parameter ranges within the context of a thermal field resulting from 3D spherical model of mantle convection. The spherical approach is essential because the structure of a thermal boundary layer is very sensitive to the curvature of the core. In this article, we point out the impact made on the phase boundary structure in the deep mantle by changing the thermodynamical parameters of the phase transition, such as the Clapeyron slope and the temperature intercept. We will also vary the amount of internal heating. Our intent is to attract interest from the mineral physics community to provide better constraints on these physical parameters of profound geophysical significance.

Model Description

There are different methods for modeling 3D spherical convection. Here, for the momentum equation, we use the classical spherical harmonic approach together with a two-point boundary-value solver for each harmonic. This combines high precision and efficiency in the treatment of depth-dependent properties. The conservation of energy is solved with a second-order finite volume method. The model lies in the anelastic approximation that preserves the thermodynamics effects related to hydrostatic compression or decompression. We have used the PREM model (16) for the bulk modulus and the background density profile. The depth dependence of the thermal expansivity is one of the most important to take into account because both the adiabatic temperature

Author contributions: M.M. and D.A.Y. designed research; M.M. performed research; and M.M. and D.A.Y. wrote the paper.

The authors declare no conflict of interest.

This article is a PNAS Direct Submission.

Abbreviations: CMB, core–mantle boundary; ppv, postperovskite.

†To whom correspondence should be addressed. E-mail: marc.monnereau@dtp.obs-mip.fr.

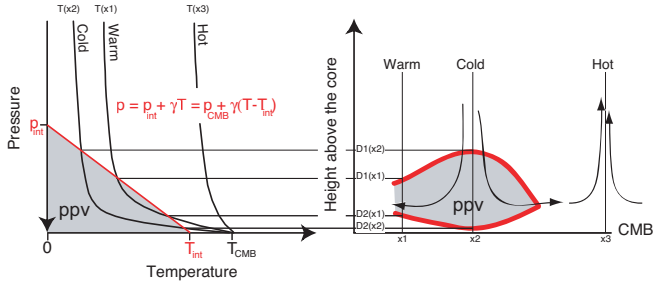

Fig. 1. Schematic diagram showing the relationship among the Clapeyron slope, the temperature intercept, T_{int}, the temperature at the CMB, T_{CMB}, and various representative thermal profiles. A double-crossing of the Clapeyron slope with the cold or warm geotherm is possible when T_{CMB} is greater than T_{int}. Hereafter, the top and bottom crossings will be referenced as D1 and D2, respectively. We note that D1and D2 should be anticorrelated. We also note that there is a narrow layer of low-velocity perovskite material under D2(x2).

gradient and the buoyancy of thermal anomalies are proportional to this parameter. Here, its radial profile is constructed in a consistent way with the variation of other properties, with the assumption of a constant Gruëneisen parameter throughout the mantle. A decrease by a factor of four of the thermal expansivity is calculated from the surface to the CMB, a value in agreement with experimental measurements for olivine (17). A description of these various profiles can be found in ref. 18 along with the development of all equations and more technical details of the model.

Besides these relatively well known mantle properties, a model of mantle convection is determined by the choice of other parameters, much less constrained, that can be considered as free parameters. T_{CMB}, the temperature at the CMB, is set at 4,000 K. This is somewhat on the high side as compared with our previous studies (18, 19) but lies within the range of the estimates of T_{CMB} (14, 20).

The thermal conductivity is both pressure- and temperature-dependent. It mainly increases with depth. Its surface value is well known, 3.3 W/mK, but the estimation for conditions at the base of the mantle is debated. It ranges between 5 W/mK and 10 W/mK (21, 22). The high value results from a linear increase throughout the mantle, but it is also suggested that the slope is proportional to the inverse of bulk modulus, leading to a flattening profile at high pressure (23). Here, we use a parabolic profile reaching 5 W/mK at the CMB.

The viscosity profile is an important constitutive element of the model because of its great influence on the average temperature. Numerous studies have attempted to portray this mantle feature, essentially from the long-wavelength geoid-topography relationship. The diversity of the proposed solutions is large, but most of them agree with a global increase with depth by one or two orders of magnitude between the upper and lower mantle. Here, the profile has two constant viscosity layers with a jump of a factor of 30 at 660 km depth. The bottom viscosity, i.e., the lower-mantle viscosity, is referred to as the reference viscosity, η.

The last free parameter is the amount of internal heating. In mantle convection modeling, this corresponds not only to the energy supplied by the radiogenic elements but also to the secular cooling. It represents the difference between the surface heat flux yielded by the convection and the heat flux released by the core. Obviously, the latter is controlled by the thermal boundary layer at the CMB. The surface heat flux is not a free parameter. It is ≈44 TW, of which only 37 TW are due to mantle convection, the remaining part being the contribution coming from the crustal radiogenic elements. Thus, to investigate the nature of the bottom boundary layer and the related D″ structure, we have performed a series of experiments where the core heat flux ranges from 10% to 50% of the total heat flux, keeping the latter at ≈37 TW. Because of the nature of the thermal boundary conditions (imposed temperature), neither the top nor the bottom heat flux can be fixed in the experiment. They are obtained by fitting the reference viscosity (decreasing the viscosity increases the vigor of the convection and the heat fluxes). This has been done for each corresponding amount of internal heating, from 50% to 90%.

Table 1 summarizes the results of the five-experiment series. The convection equations have been integrated to a quasi steady-state regime, which means many times greater than the age of the earth. For all of the calculations, we have used 128 spherical harmonics and 128 points in the radial direction.

Dynamical Effects Induced by the Postperovskite Phase Transition

Fig. 2 presents the thermal field obtained with 70% of internal heating. A few cylindrical hot plumes, surrounded by sheet-like downwellings that delineate polygons at the surface, drive the dynamics. This convective mode is the most common in 3D spherical geometry, even for large amount of internal heating (up to 90%), when the viscosity increases with depth and/or thermal expansivity decreases with depth. Besides the perovskite–ppv transition, the usual olivine to spinel and spinel to perovskite phase transitions, located at 410 and 660 km depth, are included. Their thermal effect is well visible at the head of hot plumes. Cold structures also reveal the signature of the latent heat, when they cross the endothermic barrier. This happens essentially at the junction of the downwellings, the place where they leave their 2D shape to become a more or less cylindrical structure. In contrast, no single salient thermal feature indicates the presence of the perovskite–ppv phase transition, despite a noticeable Clapeyron slope (11.5 MPa/K with a 1% density contrast).

Some previous numerical modeling (7, 9) has shown that the presence of such a strongly exothermic reaction close to the CMB destabilizes the thermal boundary layer, increasing the number of hot plumes and their time dependence. Time dependence refers here to the unstable behavior of thermal structures and the

Table 1. Summary of the results of the five-experiment series

Case	Ra	R	Lower-mantle viscosity, Pa	⟨T⟩, K	Heat power, TW				Basal heating (CMB/surface)
					Internal	Cooling	CMB	Surface	
A1	0.9×10^5	20.5	2×10^{24}	2,642	33.3	0.0	3.3	36.7	9%
A2	1.8×10^5	18.2	1×10^{24}	2,208	29.6	0.6	6.7	36.9	18%
A3	4.4×10^5	15.9	4×10^{23}	1,845	25.9	−0.1	11.7	37.5	31%
A4	7×10^5	13.7	2.5×10^{23}	1,660	22.2	−0.1	14.8	36.9	40%
A5	1.3×10^6	11.4	1.3×10^{23}	1,502	18.5	0.3	18.2	37.0	49%

The convection equations have been integrated to a quasi steady-state regime, which means many times greater than the age of the earth. For all of the calculations, we have employed 128 spherical harmonics and 128 points in the radial direction. Ra, Rayleigh number based on the lower-mantle viscosity. R, internal-heating rate. R = 12 corresponds approximately to radiogenic heating with a chondritic abundance. In the ''cooling'' column, we report the remaining derivative −dT/dt (which is positive for a cooling mantle). It is a contribution to the internal heating.

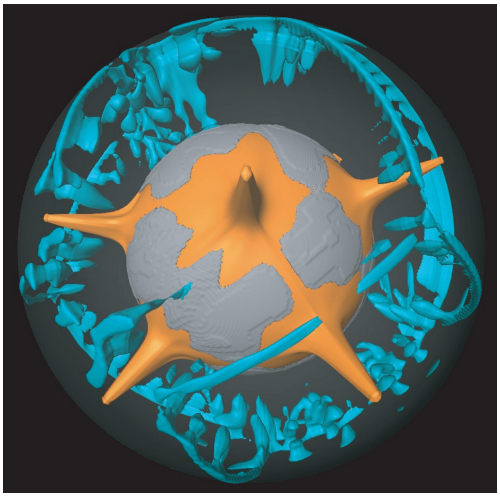

Fig. 2. Thermal field of case A3, performed with 30% of basal heating (11.5 TW from the core over 37 TW at the surface). The lower mantle is 30 times more viscous than the upper mantle. Orange, 2,500 K isotherm; blue, isosurface of the thermal anomaly of −350 K; gray, ppv lenses ($\gamma = 11.5$ MPa/K, $T_{int} = 3{,}200$ K).

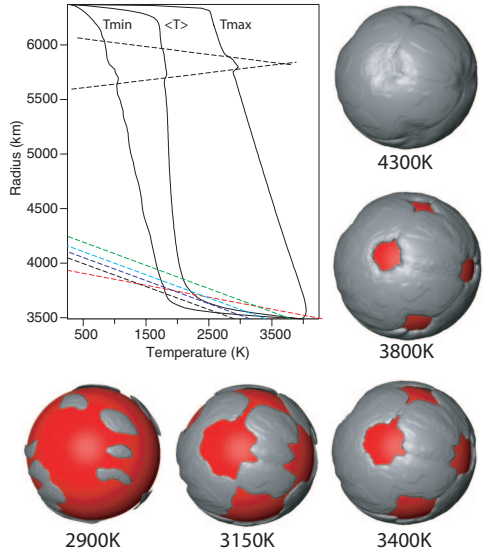

Fig. 3. Development of the surface topology of the ppv with the increasing interval between T_{int} and T_{CMB}. Shown are the three temperature profiles of case A3 (performed with 30% basal heating). The dashed lines represent the different Clapeyron curves. In black are the olivine–spinel and spinel–perovskite phase transitions. Various Clapeyron slopes for the perovskite–ppv transition have been tried. One (red) corresponds to $\gamma = 6$ MPa/K, and the others correspond to $\gamma = 11.5$ MPa/K but with different intercept temperatures T_{int} values (dark blue, 2,900 K; blue, 3,150 K; cyan, 3,400 K; green 3,800 K). At the right and below are five snapshots showing the ppv envelope (in gray) computed for each of the ppv Clapeyron curves. The surface of the core is encased in red color. The transparency regions or holes mark the perovskite lower mantle. There are two changes in the topology. For T_{int} above T_{CMB}, the ppv envelope wraps around the sphere. Below this threshold, holes (perovskite) appear around the hot plumes; they grow with increasing separation between T_{int} and T_{CMB}. When the Clapeyron curve remains below the averaged temperature profiles, the perovskite holes are connected, and the ppv envelope becomes an ensemble of distinct islands.

attendant heat flux fluctuations. This naturally results at high Rayleigh number, like the one of the earth's mantle convection. Nevertheless, these models are 2D. The reduction in the degrees of freedom is well known to accentuate the time dependence of a dynamical system. This also occurs when there is a truncation in its modal representation (24). As a matter of fact, here we do not observe any noticeable perturbation due to the presence of the ppv transition, even over the very long time scale. The time dependence only concerns the top boundary layer where the small cold structures slowly move toward the largest one while hot plumes remain nearly stationary. In 3D Cartesian geometry, Kameyama and Yuen (11) did not find an effect due to the ppv transition, except for exaggerated parameter values due to a large density change.

Topology of the Postperovskite Phase Transition

Hernlund *et al.* (4) first pointed out the fundamental difference between T_{int} above and below T_{CMB}, showing that subtle seismic signals may be interpreted in terms of "double crossing" instead of signatures involving complex structures like folded slabs (25, 26). This difference reveals topological changes in the ppv phase transition surface. We will illustrate this point by varying the interval between T_{int} and T_{CMB} in the same model. We chose the case A3 previously depicted in Fig. 2. In Fig. 3 are shown its minimum (T_{min}), horizontally averaged ($\langle T \rangle$), and maximum (T_{max}) temperature profiles with the various Clapeyron curves we used. For each curve, the model has been integrated as long as necessary to reach thermal equilibrium. The temperature profiles shown in Fig. 3 correspond to the curve with $T_{int} = 3{,}150$ K. The latent heat effect is mainly discernible on the cold profile T_{min}. The resulting ppv envelopes are shown to the right of and below the figure.

For $T_{int} > T_{CMB}$, the ppv surface entirely wraps around the core. Its surface undulates, getting closer to the CMB in the hot region, so that topographical lows coincide with the hot plume roots. The decrease of T_{int} below T_{CMB} marks a first change in topology, with the appearance of holes in the ppv layer around hot plumes. This also corresponds to a separation of the ppv from the CMB by a rather thin perovskite layer with a lower seismic velocity. In the successive snapshots in Fig. 3, holes become wider as the distance between T_{int} and T_{CMB} increases. Then, a second topological change happens when the Clapeyron curve does not cross the averaged temperature profile anymore. The holes are now connected, and the ppv envelope splits into several distinct lenses. This observation argues for the dire need to map out the D″ structure with modern seismic imaging techniques.

In Fig. 3, we have used two different Clapeyron slopes: $\gamma = 11.5$ MPa/K, recently determined by high-pressure experiments (27), and $\gamma = 6$ MPa/K, proposed earlier to fit the global D″ features from tomography models and seismic forward modeling (28). Precisely, the latter has been used here for a Clapeyron curve that just crosses the average temperature profile 250 km above the CMB, the average depth of D″. The corresponding value of T_{int} exceeds T_{CMB}.

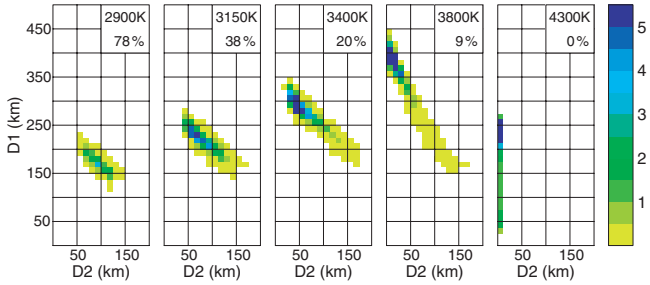

Fig. 4. The correlation map between the two surfaces where there is a phase transition crossing with the local geotherm. The ordinate and abscissa represent the heights above the CMB of the first and the second crossing, respectively (D1 and D2; see Fig. 1). Color maps out the strength of the correlation in terms of percentages subtended by the hit surface area. The last panel, where there are no holes, corresponds to $\gamma = 6$ MPa/K. Because there is no double crossing in this case, D2 has been set to zero. T_{int} and the surface percentage of "holes" are indicated in the top right corner.

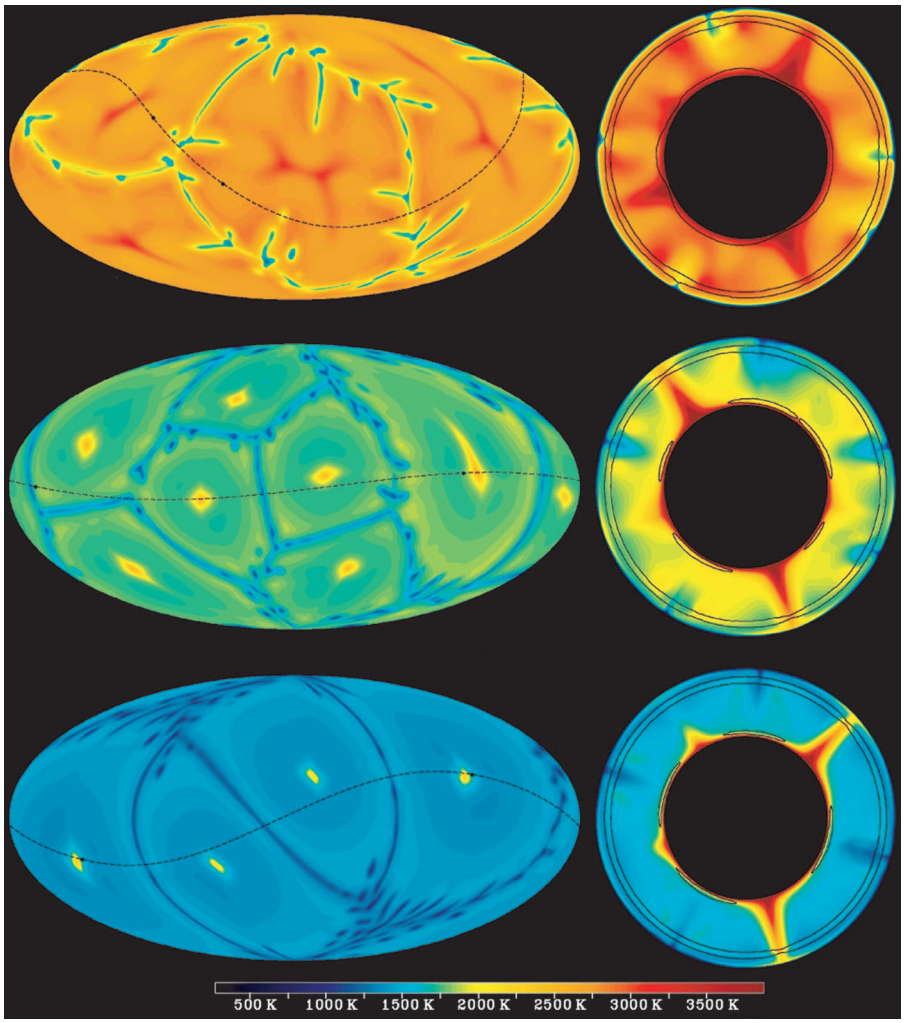

Fig. 5. Temperature field of cases A1 (*Top*), A3 (*Middle*), and A5 (*Bottom*), corresponding to 50%, 30%, and 10%, respectively, of basal heating. (*Left*) Hammer projection of a horizontal slice at mid-depth of the upper mantle. The dashed line is the trace of the radial slice presented in *Right*. On this cut, we can see the three phase transitions taken into account in the computations: the olivine–spinel ($\gamma = 3$ MPa/K), the spinel–perovskite ($\gamma = -3$ MPa/K), and close to the CMB, the perovskite–ppv ($\gamma = 11.5$ MPa/K; T_{int} has been adjusted so that the ppv horizon is 250 km thick on average).

This simply illustrates that a moderate Clapeyron slope, less than ≈6 MPa/K, would not be enough to account for both the observed average depth of D″ and the double crossing.

Fig. 4 presents a statistical approach to investigate the ppv structures. For each Clapeyron curve (and ppv surface) of Fig. 3, we build a 2D histogram that indicates the spatial correlation between both crossing heights, the top one D1 (on the ordinate) also considered as the D″ topography and the bottom one D2 (on the abscissa). The positions of D1 and D2 are illustrated in Fig. 1. Thus, at a point (D2, D1) of the histogram is plotted the area percentage of core covered by a ppv structure whose top and bottom are located at D1 and D2, respectively, above the CMB. In the case where $T_{int} > T_{CMB}$, for which there is no double crossing, we decide to set D2 (the abscissa) equal to zero. Of course, in this representation any information concerning the topology is lost. In return, the probability to find a given pair is straightforward. For instance, the double crossing (50 km, 200 km) proposed by Hernlund *et al.* (4) is not compatible with $T_{int} = 3{,}800$ K or $T_{int} = 3{,}400$ K but possible for lower values of the temperature intercept. The most important feature is the anticorrelation between D1 and D2 that is a natural consequence of the double crossing. A less obvious point concerns the slope of the correlation. It is approximately -2 for T_{int} close to T_{CMB} and tends to -1 at large distance. We may also note that the range and average depth of the top crossing (i.e., D″) reduces as the distance between T_{int} and T_{CMB} increases. Taken all together, these criteria may help to constrain some important features coming from mantle convection.

Another implication of the existence of double crossing is the inseparable presence of holes in the ppv horizon. Accordingly, a confirmation of double crossing and of the ppv origin of D″ would be to detect holes expected in the vicinity of hot plumes. The seismic signature of ppv holes should be first reflected by an absence of the D″ discontinuity. However, holes in a ppv horizon are necessarily filled with perovskite. If the holes represent a small percentage of the surface, a reference velocity model would correspond to the most abundant material at a given depth, perovskite above the average D″ depth, and ppv below. Because seismic velocities are greater in ppv than in perovskite, these holes would appear to be like slow tabular structures. They appear to be distinct just by difference in the reference model. Such a tabular slow velocity structure has been well identified beneath South Africa (29). This structure has been interpreted as evidence of a chemical pile because it is characterized by sharp and steep discontinuity (30). Looking at Fig. 3, the snapshot corresponding to $T_{int} = 3{,}800$ K exhibits very steep contours around each hole. It is not our purpose here to investigate this hypothesis in detail, but we wonder whether

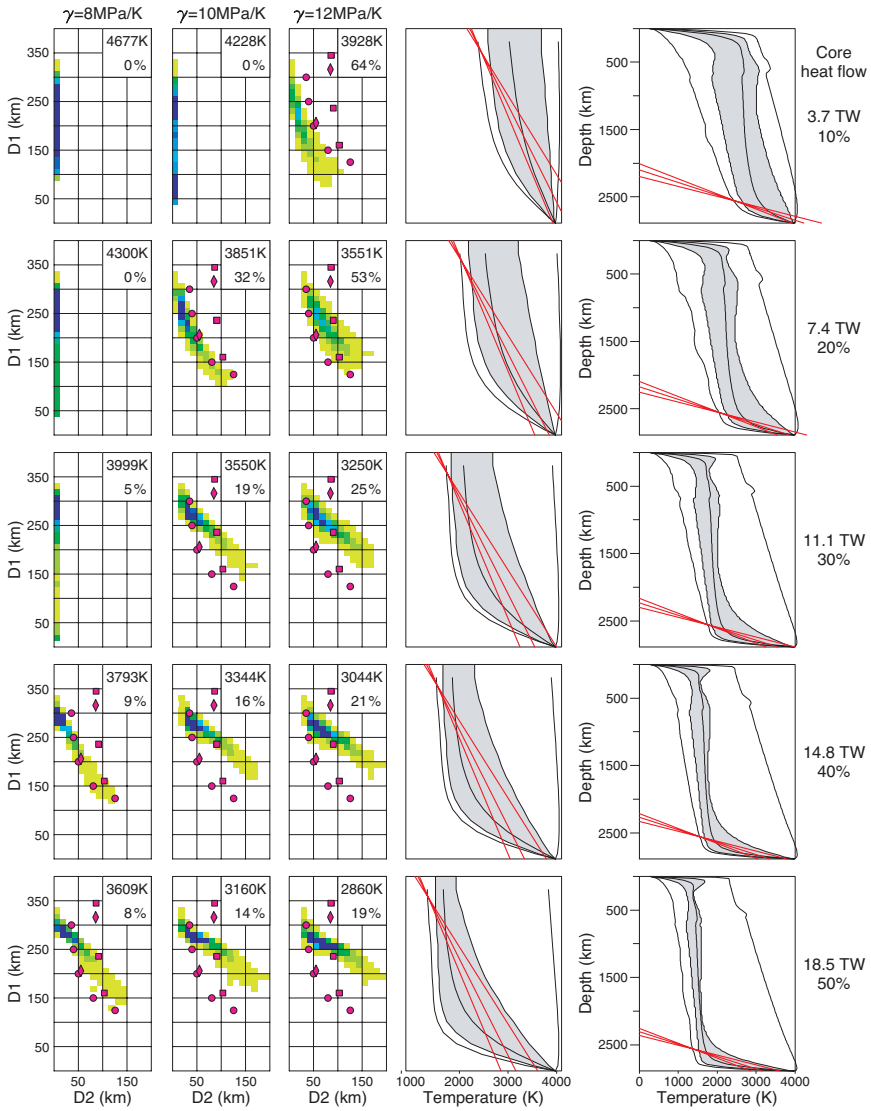

Fig. 6. Correlation maps as a function of the Clapeyron slopes (first to third columns), and the temperature profiles of models A1 to A5 (top to bottom, fourth and fifth columns). Black lines are for the minimum, averaged, and maximum temperature profiles. Ninety percent of the temperatures are inside the shaded area. The fourth column presents a zoomed-in view of the deepest 400 km of the fifth column. The red lines draw the Clapeyron curves corresponding to the first three columns. Each panel of the first three columns is a correlation map as described in Fig. 4, with $\gamma = 8$, 10, and 12 MPa/K. T_{int} has been adjusted so that the maximum of D1 is 350 km. On these diagrams, the symbols show double crossings detected beneath various area: diamonds for Eurasia (4), squares for the central Pacific (5), and circles for Central America (6). All of the diagrams are marked by an anticorrelation between D1 and D2. Only the data from Central America (circles) exhibit this feature. They are best fitted by diagrams with $\gamma = 8$ MPa/K and 40% of basal heating (first column, fourth row) or $\gamma = 10$ MPa/K and 20% of basal heating (second column, second row). Both of the fits correspond to values of T_{int} 200 K below T_{CMB}.

holes in fast layer and slow tabular structures can be distinguished. Here lies the second major consequence from the detection of double crossing.

Sensitivity to the Core Heat Flux

The D″ layer would reflect the thermal structure of the CMB that may depend on various properties, but eventually is characterized by a thickness determining the heat flux from the core. From a series of models, we investigate the sensitivity of the ppv envelope to the amount of basal heating. Fig. 5 shows three cases of this series. In all of them, hot plumes dominate the dynamics, even in case A1 where the basal heating amounts to only 10% of the surface heat flow. The global trend resulting from the comparison of these cases is a decrease of the average temperature as the amount of basal heating increases and is accompanied by a focusing of plumes and a sharpening of the temperature gradient. This feature is also well highlighted by the temperature profiles shown in Fig. 6. On these profiles, a shaded area represents 90% of the most frequent temperature around the average value. It is clearly wider in the case of large internal heating, indicating a greater variability of the thermal field.

For each case, Fig. 6 also displays three correlation maps, similar to the ones presented in Fig. 4. These correlation maps have been calculated for different Clapeyron slopes, 8, 10, and 12 MPa/K, spanning the range of values determined by recent high-pressure experiments (27, 31). Here, T_{int} has been relaxed to ensure that the maximum value of D1 is 350 km, a value representative of the highest detection of D″ above the core (32–34). The average height of D″, that is ≈250 km (32), also could have been a criterion to relax T_{int}, but less precise because the maxima of the correlation maps are fairly smooth and not well defined. It remains that this criterion may be used *a posteriori* as a global constraint of our synthetic D″ (i.e., D1).

Naturally, the main constraint is expected from double crossings. Some of them are plotted on our correlations maps. There are those proposed by Hernlund *et al.* (4) for Eurasia: (50, 200) and (80, 300). Beneath the central Pacific, Lay *et al.* (5) suggested three possible pairs, (85, 344), (90, 235), and (102, 160). Lastly, we have extracted a series of five pairs from reflectivity maps and scatter images beneath Central America (6). These images, obtained by 3D inverse scattering, exhibit two continuous widespread interfaces whose topographies are remarkably anticorrelated. As seen before, the anticorrelation provides observational evidence of the phase change. The distance between both surfaces is maximum for a pair (35, 300) and tends to zero at a merging point lying 125 km above the core. Thus, the variation of the top topography is twice the bottom one, a feature indicative of a small difference between T_{int} and T_{CMB}.

Surprisingly, double crossings from Eurasia and the central Pacific do not reveal a similar signature but a zero D1–D2 correlation in the central Pacific (D1–D2 distribution being almost vertical) and even a positive D1–D2 correlation beneath Eurasia. As a result, none of the correlation maps displayed in Fig. 6 can fit the entire data set for these regions. In contrast, the fit to the data from Central America is obvious for 40% basal heating if $\gamma = 8$ MPa/K (Fig. 6, first column, fourth row) and appears possible for 20% basal heating with γ slightly above 10 MPa/K (Fig. 6, second column, second row). Furthermore, we may suspect similar fits for other amounts of basal heating: below 8 MPa/K for 50%, between 8 and 10 MPa/K for 30%, and above 12 MPa/K for 10%. Incidentally, it is worth noting that low Clapeyron slopes, <7 MPa/K, would only be consistent with extremely high core heat flux. Thus, a univocal relation seems to exist between the Clapeyron slope and the core heat flux that explains the data from Central America, so that any improvement in the determination of the Clapeyron slope will help to reduce the uncertainty in the core heat flux.

Another remarkable point is that these solutions correspond to almost the same value of T_{int}, 150 and 200 K below T_{CMB} ($T_{\text{int}} =$ 3,851 K and $\gamma = 10$ MPa/K for 20% basal heating case; $T_{\text{int}} = 3{,}793$ K and $\gamma = 8$ MPa/K for 40% basal heating case). As noticed before, this is not a coincidence but results from the distribution of the data along a line with a slope of approximately -2. On the correlation maps of Fig. 6, this occurs only when D2 remains close to the CMB, i.e., only in the case of a small distance between T_{int} and T_{CMB}, whatever the value of the Clapeyron slope.

It still remains possible to use additional criteria to select a solution. For instance, the correlation map for $\gamma = 10$ MPa/K and 20% of core heat flux (Fig. 6, second column, second row) has a maximum for D2 around 250 km, which is in agreement with the estimated average height of D″ above the core. On the other hand, the solution with $\gamma = 8$ MPa/K and 40% of core heat flux (Fig. 6. first column, fourth row) corresponds to a model more consistent with the 1,600 K expected beneath oceanic ridges and required by the composition of mid-ocean ridge basalts. However, all of the models presented here are too simple to be able to fit all of the criteria they should respect (surface velocities, temperature of hot plumes, etc.). They simply show that double crossing offers a viable new constraint for the D″ layer.

Concluding Remarks

Previous efforts to investigate the influence of the ppv transition on mantle dynamics have overemphasized the role played by the Clapeyron slope (7–11). Our results clearly reveal that the temperature intercept, T_{int}, is also an essential determinant for describing the dynamics and topological structure of the ppv transition. The transition of the topology of the ppv envelope with increasing T_{int} to one with perovskite holes under the hot plumes has important implications because the sharp increase in seismic velocity across the boundary of the perovskite hole can be interpreted in terms of the phase transition from perovskite to ppv, instead of relying on an interpretation based on chemical heterogeneities (30). This alternative line of thinking has important ramifications for the nature of the bottom thermal boundary layer in mantle convection.

The relative position of the temperature intercept with respect to the temperature at the CMB, T_{CMB}, critically determines the presence or absence of the double-crossing effect, depending on whether T_{int} is lower or higher than T_{CMB}. A better determination of T_{int} from mineral physics will allow us to better constrain the T_{CMB}, because from ongoing improvements in seismic imaging, we are now gaining more confidence about the existence of the double-crossing phenomenon underneath subducting slabs (e.g., ref. 35). In this connection, T_{int} will also be higher with increasing amounts of Fe because Fe has the tendency of decreasing the pressure for the ppv transition to take place (36).

Our results from employing the correlation between the two phase-crossing surfaces as a constraint bring out two remarkable points. (*i*) The amount of basal heating is sensitive to the Clapeyron slope used to fit the data. For instance, a value of the Clapeyron slope around 8 MPa/K would be indicative of a large core heat flux, in the range of 15 TW, whereas a moderate core heat flux below 7.5 TW should be more relevant in the case of high Clapeyron slopes around 11.5 MPa/K. (*ii*) The distance between T_{int} and T_{CMB} should not exceed 200 K. This strongly emphasizes the importance of precise determination of the Clapeyron slope but also of the temperature intercept because both may put a strong constraint on the amount of basal heating and on the temperature of the CMB.

We thank two anonymous reviewers for their fruitful comments and Drs. Phil Allen, Stefano Baroni, Nicolas Coltice, Charley Kameyama, John Hernlund, Maarten de Hoop, Ctirad Matyska, and Renata Wentzcovitch for stimulating discussions. This work was supported by grants from the National Science Foundation programs Cooperative Studies of the Earth's Deep Interior and Information Technology Research for National Priorities. Computation support was provided by the Centre National d'Etudes Spatiales.

1. Murakami M, Hirose K, Kawamura K, Sata N, Ohishi Y (2004) *Science* 304:855–858.
2. Oganov AR, Ono S (2004) *Nature* 430:445–448.
3. Tsuchiya T, Tsuchiya J, Umemoto K, Wentzcovitch RM (2004) *Earth Planet Sci Lett* 224:241–248.
4. Hernlund JW, Thomas C, Tackley PJ (2005) *Nature* 434:882–886.
5. Lay T, Hernlund J, Garnero EJ, Thorne MS (2006) *Science* 314:1272–1276.
6. van der Hilst RD, de Hoop MV, Wang P, Shim S-H, Ma P, Tenorio L (2007) *Science* 135:1813–1817.
7. Nakagawa T, Tackley PJ (2004) *Geophys Res Lett* 31:L16611.
8. Nakagawa T, Tackley PJ (2006) *Geophys Res Lett* 33:L12S11.
9. Matyska C, Yuen DA (2005) *Earth Planet Sci Lett* 234:71–81.
10. Matyska C, Yuen DA (2006) *Phys Earth Planet Inter* 154:196–207.
11. Kameyama M, Yuen DA (2006) *Geophys Res Lett* 33:L12S10.
12. Wookey J, Stackhouse S, Kendall JM, Brodholt J, Price GD (2005) *Nature* 438:1004–1007.
13. Wentzcovitch RM, Tsuchiya T, Tsuchiya J (2006) *Proc Natl Acad Sci USA* 103:543–546.
14. Boehler R (2000) *Rev Geophys* 38:221–245.
15. Hirose K (2006) *Rev Geophys* 44:RG3001.
16. Dziewonski AM, Anderson DL (1981) *Phys Earth Planet Inter* 25:297–356.
17. Chopelas A, Boehler R (1992) *Geophys Res Lett* 19:1983–1986.
18. Monnereau M, Quere S (2001) *Earth Planet Sci Lett* 184:575–587.
19. Monnereau M, Yuen DA (2002) *Earth Planet Sci Lett* 202:171–183.
20. Jeanloz R (1990) *Annu Rev Earth Planet Sci* 18:357–386.
21. Saxena SK, Shen G, Lazor P (1994) *Science* 264:405–407.
22. Hofmeister AM (1999) *Science* 283:1699–1706.
23. Hofmeister AM (2007) *Proc Natl Acad Sci USA* 104:9192–9197.
24. Marcus PS (1981) *J Fluid Mech* 103:241–255.
25. Thomas C, Garnero EJ, Lay T (2004) *J Geophys Res Solid Earth* 109:B08307.
26. Thomas C, Kendall JM, Lowman J (2004) *Earth Planet Sci Lett* 225:105–113.
27. Hirose K, Sinmyo R, Sata N, Ohishi Y (2006) *Geophys Res Lett* 33:L01310.
28. Helmberger D, Lay T, Ni S, Gurnis M (2005) *Proc Natl Acad Sci USA* 102:17257–17263.
29. Ni SD, Tan E, Gurnis M, Helmberger D (2002) *Science* 296:1850–1852.
30. Ni SD, Helmberger DV (2003) *J Geophys Res Solid Earth* 108:2094.
31. Ono S, Oganov AR (2005) *Earth Planet Sci Lett* 236:914–932.
32. Wysession ME, Lay T, Revenaugh J, Williams Q, Garnero EJ, Jeanloz R, Kellogg LH (1998) in *The Core-Mantle Boundary Region*, eds Gurnis M, Wysession ME, Knittle E, Buffet BA (Am Geophys Union, Washington, DC), Vol 28, pp 273–297.
33. Kendall JM, Shearer PM (1995) *Phys Earth Planet Inter* 92:85.
34. Usui Y, Hiramatsu Y, Furumoto M, Kanao M (2005) *Geophys Res Lett* 32:L13311.
35. Hutko AR, Lay T, Garnero EJ, Revenaugh J (2006) *Nature* 441:333–336.
36. Mao WL, Meng Y, Shen GY, Prakapenka VB, Campbell AJ, Heinz DL, Shu JF, Caracas R, Cohen RE, Fei YW, Hemley RJ, Mao HK (2005) *Proc Natl Acad Sci USA* 102:9751–9753.